

## Article

# Broadening the Action Spectrum of TiO<sub>2</sub>-Based Photocatalysts to Visible Region by Substituting Platinum with Copper

Andrey A. Saraev , Anna Yu. Kurenkova , Evgeny Yu. Gerasimov  and Ekaterina A. Kozlova \* 

Federal Research Center, Boreskov Institute of Catalysis SB RAS, Lavrentieva Ave. 5, 630090 Novosibirsk, Russia; asaraev@catalysis.ru (A.A.S.); kurenkova@catalysis.ru (A.Y.K.); gerasimov@catalysis.ru (E.Y.G.)

\* Correspondence: kozlova@catalysis.ru

**Abstract:** In this study, TiO<sub>2</sub>-based photocatalysts modified with Pt and Cu/CuO<sub>x</sub> were synthesized and studied in the photocatalytic reduction of CO<sub>2</sub>. The morphology and chemical states of synthesized photocatalysts were studied using UV-Vis diffuse reflectance spectroscopy, high-resolution transmission electron microscopy, and X-ray photoelectron spectroscopy. A series of light-emitting diodes (LEDs) with maximum intensity in the range of 365–450 nm was used to determine the action spectrum of photocatalysts. It is shown for the first time, that the pre-calcination of TiO<sub>2</sub> at 700 °C and the use of Cu/CuO<sub>x</sub> instead of Pt allow one to design a highly efficient photocatalyst for CO<sub>2</sub> transformation shifting the working range to the visible light (425 nm). Cu/CuO<sub>x</sub>/TiO<sub>2</sub> (calcined at 700 °C) shows a rate of CH<sub>4</sub> formation of 1.2 ± 0.1 μmol h<sup>-1</sup> g<sup>-1</sup> and an overall CO<sub>2</sub> reduction rate of 11 ± 1 μmol h<sup>-1</sup> g<sup>-1</sup> (at 425 nm).

**Keywords:** photocatalysis; CO<sub>2</sub> reduction; TiO<sub>2</sub>; CH<sub>4</sub> production; visible light; ultraviolet light; copper oxides; platinum



**Citation:** Saraev, A.A.; Kurenkova, A.Y.; Gerasimov, E.Y.; Kozlova, E.A. Broadening the Action Spectrum of TiO<sub>2</sub>-Based Photocatalysts to Visible Region by Substituting Platinum with Copper. *Nanomaterials* **2022**, *12*, 1584. <https://doi.org/10.3390/nano12091584>

Academic Editors: Jose L. Hueso, Ewa Kowalska and Zhishun Wei

Received: 16 April 2022

Accepted: 5 May 2022

Published: 7 May 2022

**Publisher's Note:** MDPI stays neutral with regard to jurisdictional claims in published maps and institutional affiliations.



**Copyright:** © 2022 by the authors. Licensee MDPI, Basel, Switzerland. This article is an open access article distributed under the terms and conditions of the Creative Commons Attribution (CC BY) license (<https://creativecommons.org/licenses/by/4.0/>).

## 1. Introduction

Today, humankind faces the problem of an increase in the emission of greenhouse gases, and their utilization is increasingly becoming the actual goal. Additionally, special attention is paid to utilizing the major component of greenhouse gases—CO<sub>2</sub> [1,2]. A promising approach to utilizing CO<sub>2</sub> is its photocatalytic conversion to more reactive substances, such as CO and CH<sub>4</sub>. This technology allows reducing the amount of CO<sub>2</sub> in the atmosphere [3]. Moreover, the products of this process are organic compounds, such as methane, methanol, ethanol, and formaldehyde, which could be then converted into valuable organic components or fuels [4]. It is worth noting that such organic compounds could be synthesized using renewable sources: light, CO<sub>2</sub>, and water [5].

The thermodynamic stability and kinetic inertia of CO<sub>2</sub> limit its use in the chemical industry. The development of technologies that allow the conversion of CO<sub>2</sub> into useful organic compounds under “soft” conditions will increase the appeal of this process and facilitate its large-scale implementation. Exposure to visible or UV light irradiation is known to remove thermodynamic limitations on the reductive conversion of carbon dioxide in the presence of water into organic compounds, which makes the process of photocatalytic CO<sub>2</sub> reduction one of the most promising technologies, but the large-scale implementation of this process is hampered by the lack of effective photocatalysts.

Metal oxides, especially TiO<sub>2</sub>, are widely used as photocatalysts because of their stability and their ability to generate the electron–hole pairs under light irradiation and at a low cost [6,7]. Modification with metals allows one to enhance the activity of titania due to the separation of photogenerated charge carriers (electron–hole pairs) [8,9]. Currently, platinum is the most used metal as a cocatalyst, as it has a high working function of the electron (5.6 eV) and, therefore, promotes effective charge separation [10,11]. Despite the high activity of materials including Pt as cocatalyst, there is a necessity to develop an

effective photocatalyst with non-noble metal from a practical point of view. One of the promising cocatalysts is Cu and its oxides, both  $\text{Cu}_2\text{O}$  and  $\text{CuO}$  have narrow bandgaps and are able to absorb visible light [12–16]. It should be noted that calcination of  $\text{TiO}_2$  at high temperature leads to a shift in adsorption edge to a longer wavelength [17]. Such thermal activation should lead to enhanced photocatalytic activity under visible light irradiation. The advantage of this method is its simplicity compared with other methods for shifting the  $\text{TiO}_2$  absorption edge, such as reconstructing the  $\text{TiO}_2$  surface, embedding quantum dots, creating defects, or doping  $\text{TiO}_2$  lattice [18–22].

At the same time, although research on this process has been ongoing for the past 20 years, there is still no consensus on which photocatalysts are the most active, how the reduction of  $\text{CO}_2$  occurs, and what affects the distribution of reduction products. Most studies are aimed at the synthesis of active material for photocatalytic reduction of  $\text{CO}_2$  [3], while the identification of regularities between the nature of the products formed, as well as the rate of  $\text{CO}_2$  reduction and the state of the catalyst, facilitate the formulation of a scientific basis for creating an efficient photocatalytic system. In the case of using Cu as a cocatalyst, special attention should be paid to studying the photocatalyst surface due to the chemical versatility of Cu and the possible formation of copper oxides [23].

This research focused on a detailed study of the products of  $\text{CO}_2$  reduction that depend on the nature of surface  $\text{TiO}_2$ -based photocatalyst using Cu and Pt as cocatalysts. To explain the mechanism of the photocatalyst operation, the reduction of  $\text{CO}_2$  was studied under irradiation of light-emitting diodes with different wavelengths in the range from 365 to 450 nm, and the catalysts were characterized by transmission electron microscopy, X-ray photoelectron spectroscopy, and UV-Vis spectroscopy. In the current manuscript, the influence of Pt and Cu/ $\text{CuO}_x$ , the thermal activation of  $\text{TiO}_2$ , and the light source wavelength on the product distribution and photocatalyst activity in  $\text{CO}_2$  reduction are defined under the same conditions, for the first time. The article reveals the characteristics of the photocatalytic system that contribute to the predominant formation of  $\text{CH}_4$  during photocatalytic  $\text{CO}_2$  reduction. A simple approach involving heat treatment of  $\text{TiO}_2$  and Cu/ $\text{CuO}_x$  deposition is proposed to synthesize visible light active photocatalyst.

## 2. Materials and Methods

### 2.1. Photocatalyst Synthesis

Commercial titanium dioxide Evonik P25 (Evonik Industries AG, Essen, Germany) was used for photocatalyst preparation. Cocatalysts deposition was carried out by impregnation method using  $\text{H}_2\text{PtCl}_6$  (Reakhim, Moscow, Russia, 98%),  $\text{Cu}(\text{NO}_3)_2 \cdot 2.5\text{H}_2\text{O}$  (Reakhim, Moscow, Russia, 98%), and  $\text{NaBH}_4$  (Acros Organics, Geel, Belgium, 99%) aqueous solutions. For thermal activation,  $\text{TiO}_2$  was pre-calcined at 700 °C for 3 h. This sample is marked as “ $\text{TiO}_2$  700” in subsequent sections. Platinum and copper were deposited from aqueous solutions of  $\text{H}_2\text{PtCl}_6$  and  $\text{Cu}(\text{NO}_3)_2$  on the surface of unmodified  $\text{TiO}_2$  and  $\text{TiO}_2$  calcined at 700 °C. The synthesis is described in detail elsewhere [24,25]. The calculated metal loading was 1 wt.% and 5 wt.% for Pt and Cu, respectively.

### 2.2. Photocatalyst Characterization

The synthesized catalysts were characterized by UV-Vis diffuse reflectance spectroscopy, high-resolution transmission electron microscopy (HR TEM), inductively coupled plasma atomic emission spectroscopy, and X-ray photoelectron spectroscopy (XPS).

The diffuse reflectance UV-Vis spectra were measured using a UV-2501 PC spectrophotometer with an ISR-240A diffuse reflectance unit (Shimadzu, Kyoto, Japan).

The structure and microstructure of the photocatalysts were studied with HR TEM using a ThemisZ electron microscope (Thermo Fisher Scientific, Waltham, MA, USA) operated at an accelerating voltage of 200 kV. The microscope is equipped with a corrector of spherical aberrations, which provided a maximum lattice resolution of 0.06 nm, and a SuperX energy-dispersive spectrometer (Thermo Fisher Scientific). Images were recorded using a Ceta 16 CCD sensor (Thermo Fisher Scientific). For electron microscopy studies,

samples were deposited on perforated carbon substrates attached to aluminum grids using an ultrasonic dispersant.

Inductively coupled plasma atomic emission spectroscopy (ICP-AES) was used to perform elemental analysis of the synthesized photocatalysts. ICP-AES was carried out on an Optima 4300 5DV spectrometer (PerkinElmer Inc., Waltham, MA, USA).

The relative surface concentration of elements and their chemical states were investigated using XPS. The study was carried out using an X-ray photoelectron spectrometer (SPECS Surface Nano Analysis GmbH, Berlin, Germany), equipped with an XR-50 X-ray source and PHOIBOS-150 hemispherical electron energy analyzer. The  $Cu2p$ ,  $Pt4f$ ,  $Ti2p$ , and  $O1s$  XPS core-level spectra were recorded under ultrahigh vacuum conditions. The core-level spectra were obtained using the non-monochromatic Al  $K\alpha$  radiation ( $h\nu = 1486.61$  eV). The charge correction was performed by setting the  $Ti2p_{3/2}$  peak at 459.0 eV, which corresponded to titanium in the  $Ti^{4+}$  state of the  $TiO_2$  lattice. Relative concentrations of elements were determined from the integrated intensities of the core-level spectra using their cross-sections according to Scofield [26]. For detailed analysis, the spectra were fitted into several peaks after background subtraction using the Shirley method. The fitting procedure was performed using the CasaXPS software [27]. The line shape of the peaks was approximated by the multiplication of the Gaussian and Lorentzian functions.

### 2.3. Photocatalytic Activity Measurements

The reduction of  $CO_2$  was carried out in a batch reactor (70 mL) with a quartz window ( $16\text{ cm}^2$ ) under light irradiation (Figure 1). A suspension consisting of a catalyst (30 mg) and water (700  $\mu\text{L}$ ) was deposited on a glass support ( $8\text{ cm}^2$ ) and dried at  $50\text{ }^\circ\text{C}$  in an air atmosphere. The resulting thickness of catalyst coverage is about 100  $\mu\text{m}$ . After the deposition, the catalyst was irradiated by UV light (380 nm) for 30 min to remove organic contaminations from the photocatalyst surface and then installed in the reactor containing 1 mL of deionized water. Pure water without any additional sacrificial agents was used in all photocatalytic experiments. After that, the reactor was purged with  $CO_2$  (>99.94% purity) for 1 h. A number of light emission diodes (LEDs) with wavelength and surface power density of 365 (10  $\text{mW}/\text{cm}^2$ ), 380 (17  $\text{mW}/\text{cm}^2$ ), 400 (60  $\text{mW}/\text{cm}^2$ ), 425 (56  $\text{mW}/\text{cm}^2$ ), and 450 (42  $\text{mW}/\text{cm}^2$ ) nm was used as a light source. The surface power density was measured at the sample position.

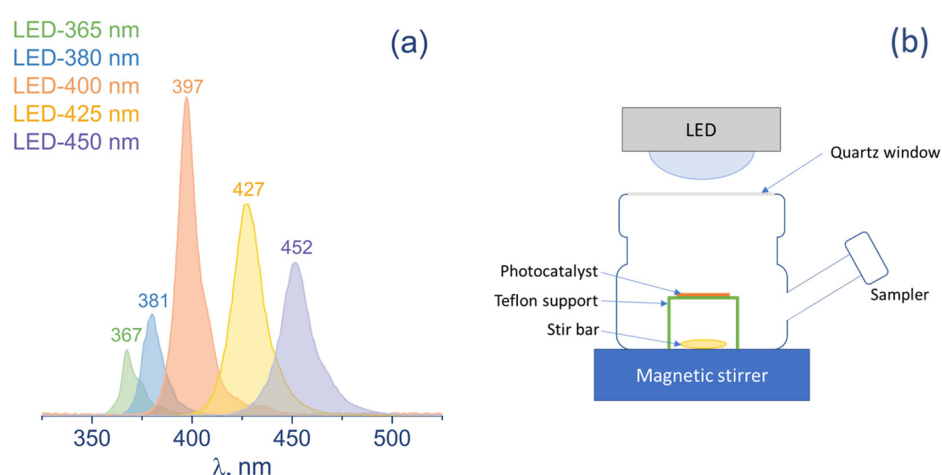


**Figure 1.** (a) Spectra of LEDs with the wavelength at maximum intensity; (b) scheme of reactor for photocatalytic study.

A kinetic experiment was carried out for 24 h. Gas probe was taken using a gas syringe (500  $\mu\text{L}$ ) and analyzed with a gas chromatograph “GH-1000” (Chromos, Moscow, Russia) equipped with the flame ionization detector and thermal conductivity detector to identify the products of  $CO_2$  reduction and  $H_2$ , respectively.

The total rate of photocatalytic CO<sub>2</sub> reduction was calculated according to the following equation:

$$W(\text{CO}_2) = \frac{8n(\text{CH}_4) + 2n(\text{CO})}{t m} \quad (1)$$

where  $n(\text{CH}_4)$  and  $n(\text{CO})$  are the amounts of CH<sub>4</sub> and CO (μmol), 2 and 8 are the coefficients for electron balance,  $t$  is the time of reaction (h), and  $m$  is the weight of photocatalyst (g).

The selectivity of CH<sub>4</sub> formation was defined as

$$S(\text{CH}_4) = \frac{8 n(\text{CH}_4)}{t m W(\text{CO}_2)} \times 100\% \quad (2)$$

The apparent quantum efficiency (AQE) was calculated according to the following equation:

$$\text{AQE} = \frac{W(\text{CO}_2)}{N_{\text{phot}}} \times 100\% \quad (3)$$

where  $N_{\text{phot}}$  is the calculated photon flux equal to 5.8 mmol h<sup>-1</sup> for LED-425.

### 3. Results and Discussion

#### 3.1. Photocatalyst Characterization

The optical properties of the synthesized photocatalysts were studied by UV-Vis diffuse reflectance spectroscopy (Figure 2a). The non-modified titania has a single, steep absorption edge around 380 nm, which is typical for Evonik (Degussa) P25. After calcination, the TiO<sub>2</sub> 700 sample demonstrates a redshift, and the absorption edge is about 400 nm. Evonik P25 is known to consist of two TiO<sub>2</sub> phases with different bandgap energy: anatase (3.2 eV) and rutile (3.0 eV) [28,29]. The observed effect indicates a structural change in TiO<sub>2</sub> during calcination and an increase in rutile content for TiO<sub>2</sub> 700. Calculated bandgap energies using Tauc plots are 3.14 eV for unmodified TiO<sub>2</sub> and 3.02 eV for TiO<sub>2</sub> 700 (Figure 2b). Earlier, it has been shown that the calcination of TiO<sub>2</sub> at 700 °C changes anatase to rutile ratio from 85:15 to 22:78 [24], which is in agreement with the UV-Vis spectroscopy study of the synthesized catalysts.

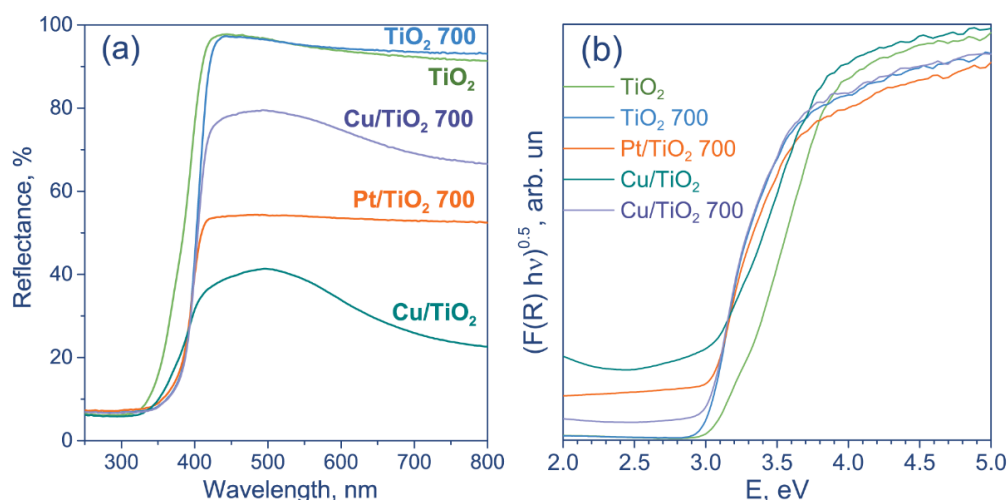


**Figure 2.** (a) Diffuse reflectance spectra of photocatalysts under study; (b) Tauc plots.

The actual metal content established by ICP-AES was around 0.7% for platinumized samples and 4.5% for Cu-containing catalysts.

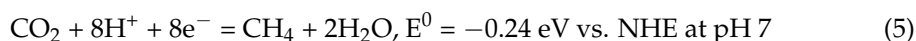
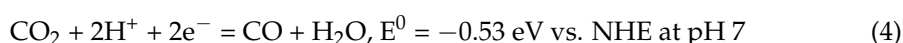
The deposition of platinum and copper promotes the adsorption of visible light for both TiO<sub>2</sub> and TiO<sub>2</sub> 700. Platinum was shown to possess a localized surface plasmon resonance in the visible region [30]. In the case of Cu-containing samples, the increased absorption is caused by the intrinsic adsorption of copper oxides due to the narrow bandgap

width of CuO (1.7 eV) and Cu<sub>2</sub>O (2.1 eV) [31,32]. The difference in the reflectance between Cu/TiO<sub>2</sub> and Cu/TiO<sub>2</sub> 700 photocatalysts may be due to the different content of CuO<sub>x</sub> and Cu since oxides enhance the light absorption of the samples, whereas metal Cu does not [33]. Adsorption beyond 600 nm is related to the bandgap transitions of CuO [12]. We speculated that the content of CuO in Cu/TiO<sub>2</sub> is higher than in Cu/TiO<sub>2</sub> 700, which was further confirmed by HR TEM and XPS.

### 3.2. Kinetic Experiments

The activity of the synthesized photocatalysts was studied in the reduction of CO<sub>2</sub> using a series of LEDs with an intensity maximum at about 365, 380, 400, 425, and 450 nm as light sources to define the spectrum of action of photocatalysts.

Since H<sub>2</sub>O was added to the studied system, the following processes could proceed on the photocatalyst surface [8,34]:



The products of reactions were analyzed using gas chromatography: CO and CH<sub>4</sub> were the main products, and H<sub>2</sub> was detected in negligible amount—less than 0.05 μmol after 24 h of reaction for the most active catalyst, i.e., Cu/TiO<sub>2</sub>.

The rates of CO, CH<sub>4</sub> formation, and total CO<sub>2</sub> reduction are presented in Figure 3. One can see that the Pt deposition changes the distribution of products and greatly increases the amount of CH<sub>4</sub>. The Pt/TiO<sub>2</sub> and Pt/TiO<sub>2</sub> 700 samples predominantly reduce CO<sub>2</sub> to CH<sub>4</sub>, and only a little amount of CO is detected, except for the LED-450 nm. When using Cu-containing samples, the dependence is more complex. Under UV irradiation, the formation rates of CO are higher than those of CH<sub>4</sub>. Nevertheless, the amounts of CH<sub>4</sub> produced over Cu/TiO<sub>2</sub> and Cu/TiO<sub>2</sub> 700 are similar to those for Pt/TiO<sub>2</sub>. At the same time, Cu/TiO<sub>2</sub> and Cu/TiO<sub>2</sub> 700 yield CO at significantly higher rates than Pt/TiO<sub>2</sub>, resulting in a higher overall CO<sub>2</sub> reduction efficiency. The activity of these photocatalysts is close to that of Pt/TiO<sub>2</sub> 700 under LED-365 nm, which demonstrates that the highest rate of overall CO<sub>2</sub> reduction under UV light is equal to  $2.8 \pm 0.3 \mu\text{mol h}^{-1} \text{g}^{-1}$ .

According to UV-Vis spectra, all photocatalysts exhibit strong light absorption at a wavelength of 365 nm. However, with an increase in the wavelength to 380 nm, the absorption of the samples obtained without preliminary calcination of TiO<sub>2</sub> decreases compared with the calcined samples. Pt/TiO<sub>2</sub> 700 demonstrates higher activity under LED-380 nm and LED-365 nm, compared with Pt/TiO<sub>2</sub>. Therefore, the difference in activity between Pt/TiO<sub>2</sub> and Pt/TiO<sub>2</sub> 700 is not caused only by different light absorption. The most likely reason for the improved activity under UV light is the increased lifetime of photogenerated charge carriers—electrons and holes—for Pt/TiO<sub>2</sub> 700 due to the efficient transfer of photogenerated electrons from TiO<sub>2</sub> to metal particles. To clarify the reason for the increased activity of the Pt/TiO<sub>2</sub> 700 sample under irradiation with LED-365 nm, compared with Pt/TiO<sub>2</sub>, the photocatalysts were characterized using HR TEM and XPS.

The HR TEM micrographs of the Pt/TiO<sub>2</sub> and Pt/TiO<sub>2</sub> 700 are presented in Figure 4. For Pt/TiO<sub>2</sub>, one can identify well-crystallized TiO<sub>2</sub> nanoparticles with a size of 10–25 nm (Figure 4a), whereas in the case of Pt/TiO<sub>2</sub> 700 catalyst (Figure 4b), the average size of crystallized TiO<sub>2</sub> nanoparticles increases to about 35–45 nm. The effect of thermal treatment has been previously studied and shown to lead to a decrease in the specific surface area of the TiO<sub>2</sub> support, an increase in crystallite size, and the part of rutile [24]. It should be noted that, for both supports, the platinum nanoparticles have a narrow particle size distribution, with mean particle sizes of 1.9 and 2.2 nm for Pt/TiO<sub>2</sub> and Pt/TiO<sub>2</sub> 700, respectively. The difference between these catalysts is the aggregates of Pt nanoparticles observed in the case of Pt/TiO<sub>2</sub>. For Pt/TiO<sub>2</sub> 700, Pt nanoparticles are well distributed on the TiO<sub>2</sub> surface and do not form agglomerate structures.

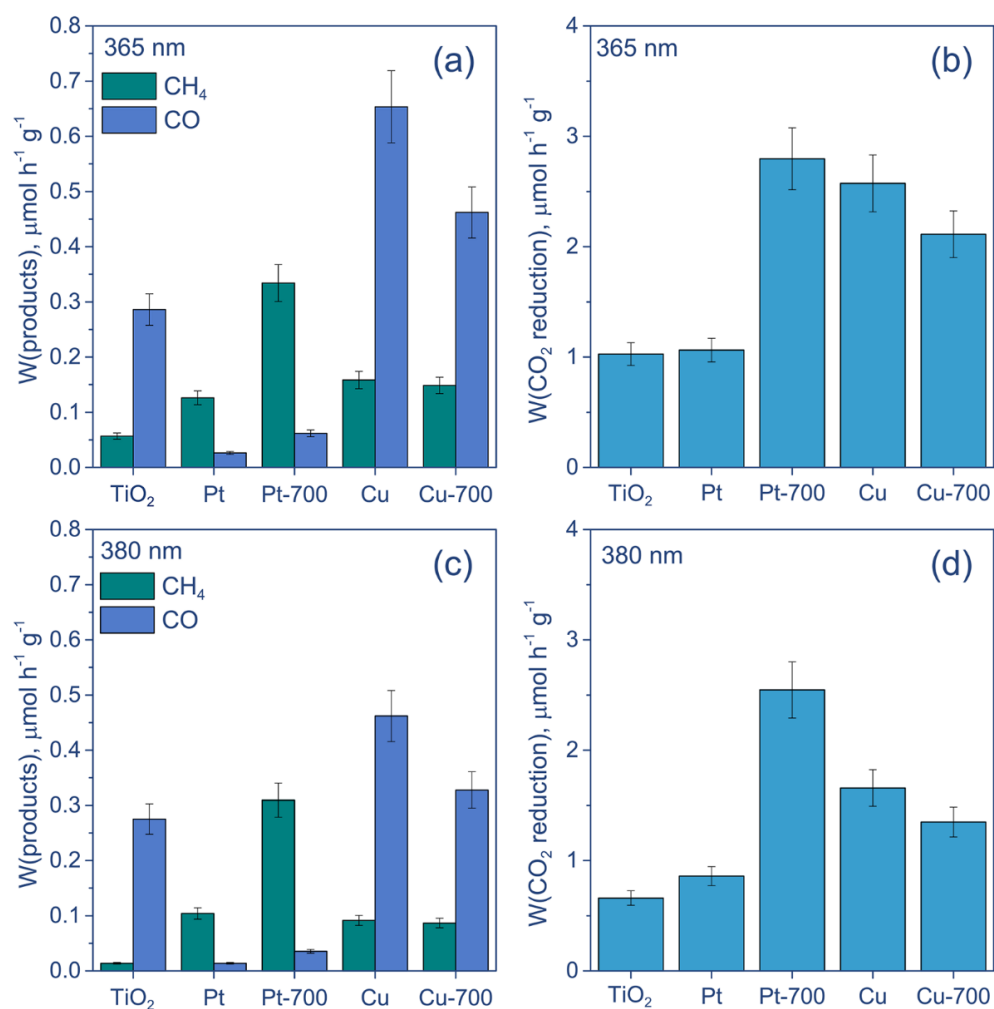


**Figure 3.** The results of activity study of photocatalytic reduction of CO<sub>2</sub> under irradiation by light of (a,b) LED-365 nm and (c,d) LED-380 nm. Conditions:  $m(\text{cat.}) = 30 \text{ mg}$ ,  $P_0(\text{CO}_2) = 1 \text{ atm}$ ,  $t = 24 \text{ h}$ . Designation: “Pt” and “Cu” means Pt/TiO<sub>2</sub> and Cu/TiO<sub>2</sub>, respectively; “Pt-700” and “Cu-700” means Pt/TiO<sub>2</sub> 700 and Cu/TiO<sub>2</sub> 700, respectively.

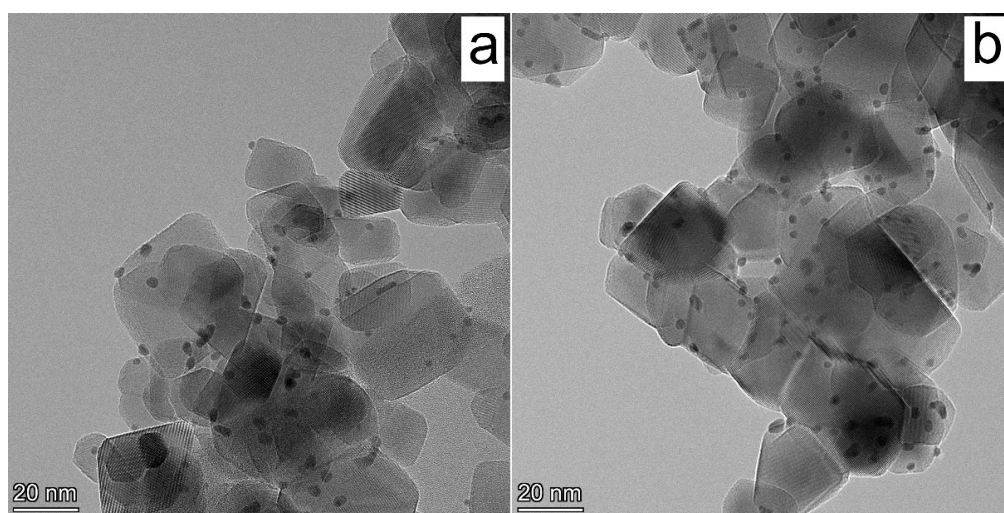


**Figure 4.** HR TEM micrographs of (a) fresh Pt/TiO<sub>2</sub> and (b) Pt/TiO<sub>2</sub> 700 photocatalysts.

The XPS study of the Pt/TiO<sub>2</sub> and Pt/TiO<sub>2</sub> 700 samples revealed that the [Pt]/[Ti] ratio in the Pt/TiO<sub>2</sub> 700 photocatalyst increases by a factor of two, compared with Pt/TiO<sub>2</sub> (Table 1). This effect is caused by a decrease in the surface area of TiO<sub>2</sub>, as shown in our previous research [24]. Since the thermal treatment of TiO<sub>2</sub> was carried out in the same manner, we assumed a similar change in surface area. The binding energy of the Pt4f<sub>7/2</sub> peak is 70.9 eV for both catalysts, which corresponds to platinum in the metallic state (Figure S1a). Additionally, these samples were studied using XPS after a photocatalytic reaction under LED-400 nm, and no change in the state of Pt was observed (Figure S1b). The [O]/[Ti] ratio after calcination of the initial TiO<sub>2</sub> sample and after carrying out the photocatalytic reaction almost does not change. This small increase could be related to the formation of cation vacancies in a negligible amount [35]. Thus, the higher activity of Pt/TiO<sub>2</sub> 700 is due to the high surface concentration of platinum nanoparticles and enhanced absorption properties of calcinated TiO<sub>2</sub>.

**Table 1.** Relative atomic concentrations of elements in the surface area of the catalysts under study and Pt4f<sub>7/2</sub> and O1s binding energies.

Sample	[Pt]/[Ti]	[O]/[Ti]	Binding Energy, eV	
			Pt4f <sub>7/2</sub>	O1s
Pt/TiO <sub>2</sub>	0.009	2.50	70.9 (Pt <sup>0</sup> )	530.3
Pt/TiO <sub>2</sub> 700	0.020	2.53	70.9 (Pt <sup>0</sup> )	530.3
Pt/TiO <sub>2</sub> (LED-400 nm)	0.009	2.51	70.8 (Pt <sup>0</sup> )	530.3
Pt/TiO <sub>2</sub> 700 (LED-400 nm)	0.016	2.56	70.9 (Pt <sup>0</sup> )	530.3

Under light irradiation with a maximum intensity at 400 nm, both Cu-containing photocatalysts demonstrate higher CH<sub>4</sub> formation rates than CO (Figure 5a). Moreover, their activities are much higher than that of both platinized samples and achieve  $37 \pm 4$  and  $31 \pm 3 \mu\text{mol h}^{-1} \text{g}^{-1}$  for Cu/TiO<sub>2</sub> and Cu/TiO<sub>2</sub> 700, respectively (Figure 5b). When using LED-425 nm, the activity of photocatalysts based on calcinated TiO<sub>2</sub> (Pt/TiO<sub>2</sub> 700 and Cu/TiO<sub>2</sub> 700) exceeds the activity of photocatalysts based on uncalcinated TiO<sub>2</sub> (Figure 5c,d). Additionally, Cu/TiO<sub>2</sub> produces more CO than CH<sub>4</sub>, while Cu/TiO<sub>2</sub> 700 is still more active toward CH<sub>4</sub> formation. Finally, the use of LED-450 nm leads to the predominant formation of CO for all studied catalysts, but the efficiency of this process is low (Figure 5e,f). Nevertheless, calcined photocatalysts are still more active in overall CO<sub>2</sub> reduction, with a reaction rate of about  $1 \mu\text{mol h}^{-1} \text{g}^{-1}$ .

The calcinated samples have a shifted adsorption edge, compared with unmodified ones and, therefore, enhanced absorption and improved photocatalytic activity under visible light (425 and 450 nm). Since the dependence under LED-400 nm is more complex, the Cu-containing samples were studied using XPS and HR TEM in the high-angle annular dark-field scanning mode (HAADF STEM). The HAADF STEM allows one to make micrographs of samples with high contrast, with the bright area corresponding to the atoms with higher Z.

The HAADF STEM micrographs of the Cu/TiO<sub>2</sub> and Cu/TiO<sub>2</sub> 700 are presented in Figure 6. For Cu/TiO<sub>2</sub>, one can see that copper nanoparticles have a wide particle size distribution in the range of 1.5–5 nm, whereas, in the case of Cu/TiO<sub>2</sub> 700, a narrow particle size distribution in the range of 1–2 nm is found. It is worth noting that, in the case of Cu/TiO<sub>2</sub> 700, the agglomerates of Cu nanoparticles are not observed. Moreover, in the case of Cu/TiO<sub>2</sub>, the EDX mapping reveals the presence of massive Cu particles of 200–400 nm (Figure S2a). Thus, the use of calcined TiO<sub>2</sub> as support allows the synthesis of a photocatalyst with a fine size distribution of Cu nanoparticles.

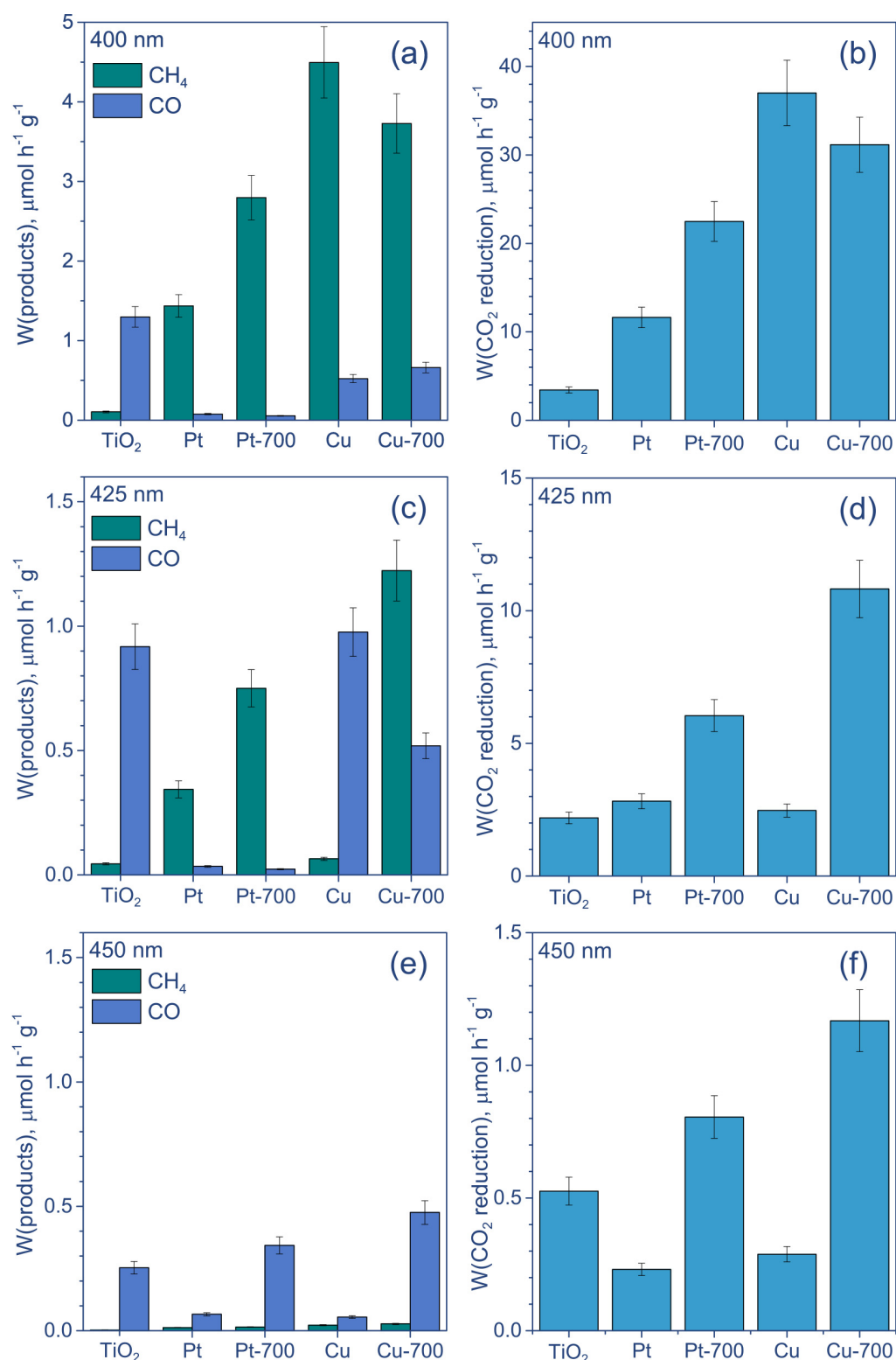


**Figure 5.** The results of activity study of photocatalytic reduction of CO<sub>2</sub> under irradiation by light of (a,b) LED-400 nm, (c,d) LED-425 nm, and (e,f) LED-450 nm. Conditions:  $m(\text{cat.}) = 30 \text{ mg}$ ,  $P_0(\text{CO}_2) = 1 \text{ atm}$ ,  $t = 24 \text{ h}$ . Designation: “Pt” and “Cu” means Pt/TiO<sub>2</sub> and Cu/TiO<sub>2</sub>, respectively; “Pt-700” and “Cu-700” means Pt/TiO<sub>2</sub> 700 and Cu/TiO<sub>2</sub> 700, respectively.

According to the results of UV-Vis spectroscopy, Cu/TiO<sub>2</sub> and Cu/TiO<sub>2</sub> 700 absorb visible light to varying degrees, but light absorption in this region indicates the presence of copper oxides in both samples. This assumption was clearly confirmed by the XPS study

(Table 2). According to the XPS analysis, the fraction of  $\text{Cu}^{2+}$  cations is about 78% and 52% for  $\text{Cu}/\text{TiO}_2$  and  $\text{Cu}/\text{TiO}_2$  700, respectively (Figure S3a). However, it should be stressed that the identification of  $\text{Cu}^{1+}$  and  $\text{Cu}^0$  states by analyzing the  $\text{Cu}2p$  spectrum is difficult, as the  $\text{Cu}2p_{3/2}$  binding energies of  $\text{Cu}^{1+}$  and  $\text{Cu}^0$  states are similar [36]. Nevertheless, the Auger parameter  $\alpha$ , which is equal to the sum of the  $\text{Cu}2p_{3/2}$  peak binding energy and the  $\text{Cu}$   $LMM$  peak kinetic energy, can be used for the identification of  $\text{Cu}^{1+}$  and  $\text{Cu}^0$  states. Unfortunately, the surface concentration of copper cations did not allow us to measure the  $\text{Cu}$   $LMM$  peak kinetic energy and identify the cation distribution. It should also be noted that the  $[\text{Cu}]/[\text{Ti}]$  surface ratios are slightly different for  $\text{Cu}/\text{TiO}_2$  and  $\text{Cu}/\text{TiO}_2$  700. The observed deviation is explained by the surface sensitivity of XPS, which is affected by different size distributions of copper nanoparticles, the presence of large  $\text{Cu}/\text{CuO}_x$  particles (in the case of  $\text{Cu}/\text{TiO}_2$ ), and a decrease in the surface area of  $\text{TiO}_2$ . Although the presence of  $\text{CuO}_x$  is beneficial for light absorption in the visible region, due to the agglomeration of copper nanoparticles and the presence of large  $\text{Cu}/\text{CuO}_x$  particles in the sample  $\text{Cu}/\text{TiO}_2$  (Figure S2a),  $\text{Cu}/\text{TiO}_2$  cannot work as efficiently as the  $\text{Cu}/\text{TiO}_2$  700 photocatalyst. The study of catalysts after irradiation by LED-400 nm and LED-450 nm does not reveal any significant changes in  $\text{Cu}/\text{TiO}_2$  700 (Figure S3b) when the  $[\text{Cu}]/[\text{Ti}]$  surface ratio decreases in the case of  $\text{Cu}/\text{TiO}_2$ . Moreover, the XPS analysis of  $\text{Cu}/\text{TiO}_2$  700 after 120 h of irradiation by LED-400 nm clearly demonstrates its stability.

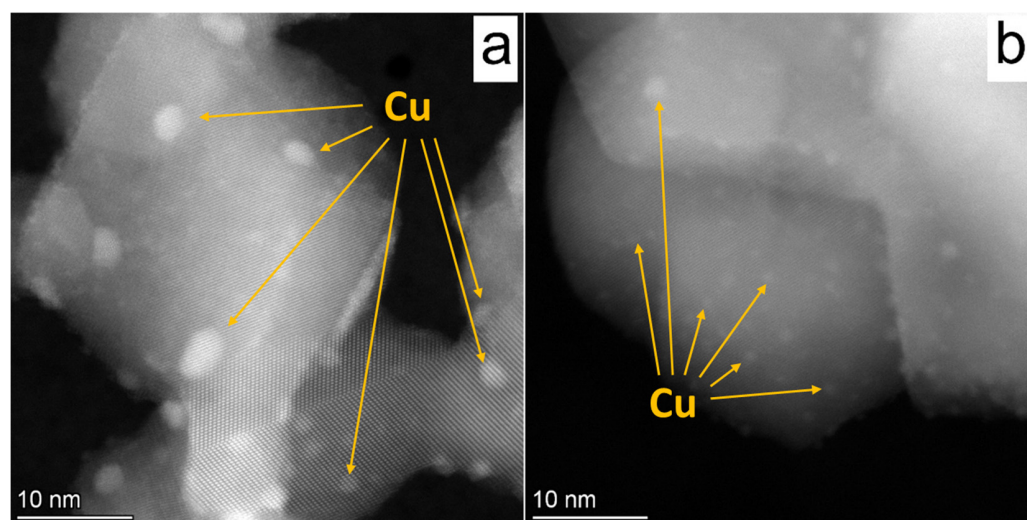


**Figure 6.** HAADF STEM micrographs of (a) fresh  $\text{Cu}/\text{TiO}_2$  and (b)  $\text{Cu}/\text{TiO}_2$  700 photocatalysts. The arrows indicate the copper nanoparticles. The bright area corresponds to copper atoms.

**Table 2.** Atomic ratios of elements in the surface layer of samples  $\text{Cu}/\text{TiO}_2$  and  $\text{Cu}/\text{TiO}_2$  700 before and after photocatalytic reaction. In parentheses is the diode that was used to carry out the reaction in the case of samples tested.

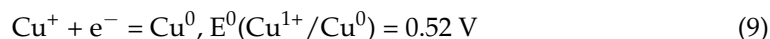
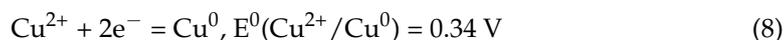
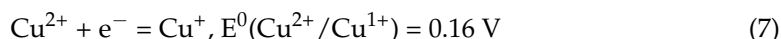
Sample	$[\text{Cu}]/[\text{Ti}]$ <sup>1</sup>	$[\text{Cu}^*]/[\text{Ti}]$ <sup>2</sup>	$[\text{O}]/[\text{Ti}]$	$\text{Cu}^*$ , % <sup>2</sup>	$\text{Cu}^{2+}$ , %
$\text{Cu}/\text{TiO}_2$	0.28	0.06	2.64	22	78
$\text{Cu}/\text{TiO}_2$ 700	0.20	0.10	2.66	48	52
$\text{Cu}/\text{TiO}_2$ (400 nm)	0.26	0.05	2.63	18	82
$\text{Cu}/\text{TiO}_2$ (450 nm)	0.22	0.05	2.61	25	75
$\text{Cu}/\text{TiO}_2$ 700 (400 nm)	0.20	0.08	2.71	41	59
$\text{Cu}/\text{TiO}_2$ 700 (450 nm)	0.26	0.08	2.66	32	68
$\text{Cu}/\text{TiO}_2$ 700 (400 nm, 120 h of reaction)	0.19	0.11	2.63	57	43

<sup>1</sup>  $\text{Cu}$ —total  $\text{Cu}$  in all states ( $\text{Cu}^0$ ,  $\text{Cu}^{1+}$ , and  $\text{Cu}^{2+}$ ); <sup>2</sup>  $\text{Cu}^*$ — $\text{Cu}$  in the states  $\text{Cu}^0$  and  $\text{Cu}^{1+}$ .

Based on the kinetic results and the photocatalyst characterization, we can speculate that the product distribution of the CO<sub>2</sub> reduction process depends on the nature of the cocatalyst and the optical absorption edge of the photocatalyst. Provided that there is enough energy of photons for the generation of a relatively high number of electrons, electrons can be collected in a cocatalyst and participate in the multi-electron process of CO<sub>2</sub> reduction to CH<sub>4</sub> (Equation (3)) [37]. The photon energy required could be reduced by depositing a cocatalyst, which can absorb light with a longer wavelength, and/or by changing the adsorption edge of TiO<sub>2</sub>. The combination of these two approaches makes it possible to obtain a photocatalyst exhibiting high activity with respect to methane under irradiation with 425 nm wavelength. The formation rate of CH<sub>4</sub> over the Cu/TiO<sub>2</sub> 700 sample achieves  $1.2 \pm 0.1 \mu\text{mol h}^{-1} \text{g}^{-1}$  and an overall CO<sub>2</sub> reduction rate of  $11 \pm 1 \mu\text{mol h}^{-1} \text{g}^{-1}$  (for a LED-425 nm). A possible reason for the low CH<sub>4</sub> formation rate over Cu/TiO<sub>2</sub> and Cu/TiO<sub>2</sub> 700 when using LEDs with a wavelength of 365 and 380 nm is the different electron surface densities in the photocatalyst. Since TiO<sub>2</sub> has strong adsorption in the UV region, it can effectively generate electron–holes pairs under LED-365 and LED-380. It has been shown that CO<sub>2</sub> reduction on the TiO<sub>2</sub> surface predominantly led to CO formation [38]. Under visible light irradiation, copper oxides absorb light to a much greater extent than TiO<sub>2</sub>, therefore, the main generation of charge carriers occurs in cocatalyst particles (Cu/CuO<sub>x</sub>), and the most of the electrons are located in the metal, which leads to an increase in the rate of methane formation [39].

The photocatalytic activity of Cu/TiO<sub>2</sub> 700 at 425 nm is caused by several factors. Firstly, the absorption edge of the sample is around 400 nm, but since the light absorption of TiO<sub>2</sub> 700 decreases gradually from 330 to 440 nm, the photocatalyst is still able to absorb light irradiation beyond 400 nm, although to a lesser extent. Additionally, since LEDs have non-monochromatic radiation, LED-425 emits light with a wavelength of both more and less than 425 nm, as shown in Figure 1a. Finally, the presence of CuO<sub>x</sub> greatly promotes the adsorption of visible light, as stated in the Introduction section. We believe that the observed behavior of Cu/TiO<sub>2</sub> 700 will promote the use of Cu-TiO<sub>2</sub>-based catalysts for the conversion of CO<sub>2</sub> under visible light.

Additionally, it should be noted that the fraction of Cu<sup>2+</sup> and Cu<sup>0</sup>/Cu<sup>1+</sup> cations varies after the photocatalytic reaction for both the Cu/TiO<sub>2</sub> and Cu/TiO<sub>2</sub> 700 catalysts (Table 2). This behavior indicates that copper cations play key roles in the reduction of CO<sub>2</sub> and could influence product distribution. The photogenerated electrons could reduce the copper oxides according to the following equations [40]:



while the reduced states could be oxidized by the free oxygen anion radicals generated due to the reaction of O<sub>2</sub> with e<sup>−</sup> (Equation (10)) or by singlet oxygen, which is the product of a reaction between O<sub>2</sub><sup>−</sup> and h<sup>+</sup> (Equation (11)) [41].



Therefore, ternary heterostructures, including Cu, CuO<sub>x</sub>, and TiO<sub>2</sub>, can be formed during the photocatalytic reaction. Both CuO<sub>x</sub> and TiO<sub>2</sub> compounds adsorb light irradiation and generate electron–hole pairs. CuO (p-type) and TiO<sub>2</sub> (n-type) form a p–n heterojunction, and the electron transfer from TiO<sub>2</sub> to CuO suppresses the charge recombination [42–44]. The charge separation between TiO<sub>2</sub> and Cu<sub>2</sub>O is realized according to the Z-scheme, according to which electrons from the conduction band (CB) of TiO<sub>2</sub> recombine with holes from the valence band of Cu<sub>2</sub>O [45]. The CB of Cu<sub>2</sub>O is  $-1.55 \text{ eV}$  [46], which is much lower than the potential of CO<sub>2</sub> reduction to CO and CH<sub>4</sub> in the presence of water

(Equations (2) and (3)). Therefore, the remaining electrons in  $\text{Cu}_2\text{O}$  can easily react with  $\text{CO}_2$  to produce  $\text{CO}$  or  $\text{CH}_4$ . At the same time, holes in  $\text{TiO}_2$  react with water vapor. The working function of  $\text{Cu}$  is higher than that of  $\text{TiO}_2$  and  $\text{CuO}_x$ ; therefore, the presence of metallic  $\text{Cu}$  promotes electron transfer to metal particles from  $\text{TiO}_2$ , as well as from  $\text{CuO}_x$ , thus improving the charge separation and the lifetime of  $e^-$  and  $h^+$  [47–50]. Depending on the position of copper and which contacts are present in the catalyst ( $\text{Cu-TiO}_2$ ,  $\text{Cu-CuO}_x$ , or both of them), various mechanisms for the transfer of photogenerated charge carriers can be realized. This is a difficult task and requires another detailed study, for example, in situ/operando X-ray absorption spectroscopy (XAS) study of  $\text{Cu}$   $K$ -edge during the photoreduction of  $\text{CO}_2$ . It should be noted that XAS is more sensitive to the oxidation states of copper cations than XPS and allows the  $\text{Cu}^{2+}$ ,  $\text{Cu}^{1+}$ , and  $\text{Cu}^0$  states to be easily distinguished [51].

### 3.3. Stability Test

To study the catalytic stability of the most active catalyst ( $\text{Cu/TiO}_2$  700), stability tests were carried out. The activity of  $\text{Cu/TiO}_2$  700 catalyst was tested during five 24 h runs under irradiation of LED-400 nm (Figure 7). Between the runs, light irradiation was turned off, and the reactor was purged with  $\text{CO}_2$  for 1 h.

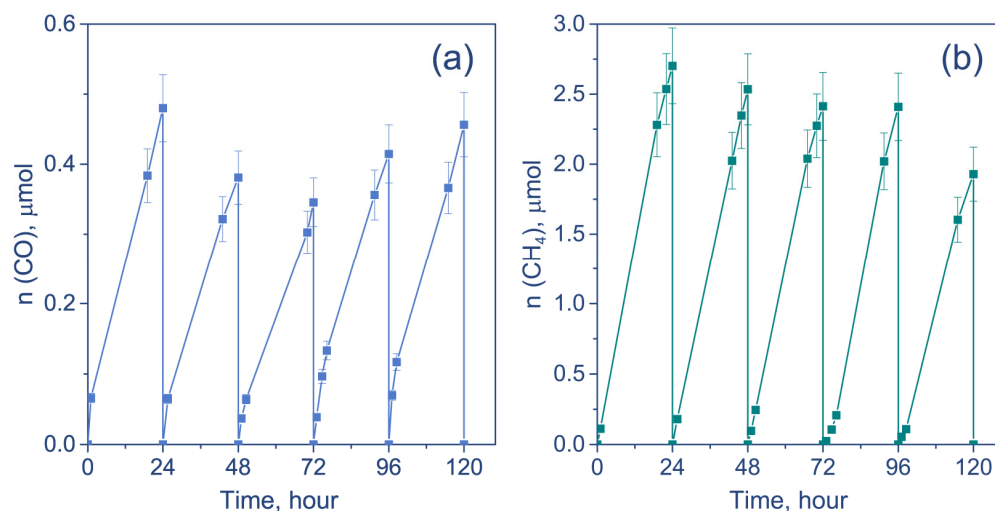


**Figure 7.** The amounts of (a)  $\text{CO}$  and (b)  $\text{CH}_4$  formed during the stability test. Conditions:  $m(\text{cat.}) = 30 \text{ mg}$ ,  $P_0(\text{CO}_2) = 1 \text{ atm}$ ,  $t$  (1 run) = 24 h,  $\lambda = 400 \text{ nm}$ .

The  $\text{CO}$  formation rate slightly decreases during the second and third runs and then begins to grow; the rate of  $\text{CH}_4$  formation stays constant throughout the first four runs and then decreases. In general, the photocatalyst exhibits high stability during 120 h of  $\text{CO}_2$  reduction. The total amount of  $\text{CH}_4$  is  $400 \mu\text{mol g}^{-1}$  and, for  $\text{CO}$ , is  $70 \mu\text{mol g}^{-1}$  after 120 h of irradiation. The observed decrease in photocatalytic activity could be due to the decrease in the number of active centers. It was mentioned above that eight electrons are necessary to convert  $\text{CO}_2$  to  $\text{CH}_4$ , whereas for  $\text{CO}$  production, two electrons are needed. Thus, the decrease in the number of heterojunctions could lead to a shift in the rate of  $\text{CO}_2$  reduction to  $\text{CO}$ . It is likely that a decrease in the number of active centers is due to the increased size of copper nanoparticles. It is known that copper oxides could undergo photocorrosion caused by photoelectron reduction [52]. It has been previously observed that the reduction of transition metal oxides to the metallic phase could lead to the migration of metallic nanoparticles over the surface and the formation of metallic agglomerates [53,54]. The formation of agglomerates could lead to a decrease in the number of active sites and, thus, a decrease in photocatalytic activity. We believe that the calcination of  $\text{TiO}_2$  leads to the formation of sites where the copper nanoparticle could be fixed, so as not to allow them to migrate over the surface and form the agglomerates. Indeed, as it was mentioned above,

the EDX mapping shows that, in the case of Cu/TiO<sub>2</sub> catalyst, the agglomerates of copper nanoparticles are found, as well as large copper particles of 100–200 nm (Figure S2a). At the same time, the EDX analysis does not reveal any copper particles of 10–100 nm in the case of Cu/TiO<sub>2</sub> 700 catalysts (Figure 8a). The stabilization of nanoparticles, which prevents the aggregation of Cu/CuO<sub>x</sub> nanoparticles on the support, is the key to increasing the long-term stability of photocatalysts. Additionally, the EDX analysis of Cu/TiO<sub>2</sub> catalyst exposed under LED-450 nm for 24 h reveals an increase in the number of copper particles with sizes of 100–200 nm (Figure S2b,c). To investigate its long-term stability, the Cu/TiO<sub>2</sub> 700 catalyst was studied using EDX after the fifth run of CO<sub>2</sub> reduction under irradiation of LED-400 nm (Figure 8b). One can see two regions enriched with Cu. The size of these agglomerates is about 20 nm, and that is much lower than Cu particles observed after 24 h of irradiation of Cu/TiO<sub>2</sub> (Figure S2c). Additionally, the distribution of oxygen (Figure S4a,b) in Cu/TiO<sub>2</sub> 700 after five runs indicates the absence of an area enriched with O at the place of Cu atom agglomeration. It can be concluded that this region, enriched in Cu atoms, mainly consists of metallic copper. Such metallic particles can be formed by the migration of metallic nanoparticles due to the reduction of copper oxides, as mentioned above. Therefore, the decrease in CH<sub>4</sub> production clearly observed on the fifth run could be caused by the agglomeration of Cu/CuO<sub>x</sub> particles, thus decreasing contact between cocatalyst and TiO<sub>2</sub> particles and reducing the lifetime of electrons. Additionally, the reduction of CuO<sub>x</sub> to Cu decreases the visible light absorption by photocatalyst.

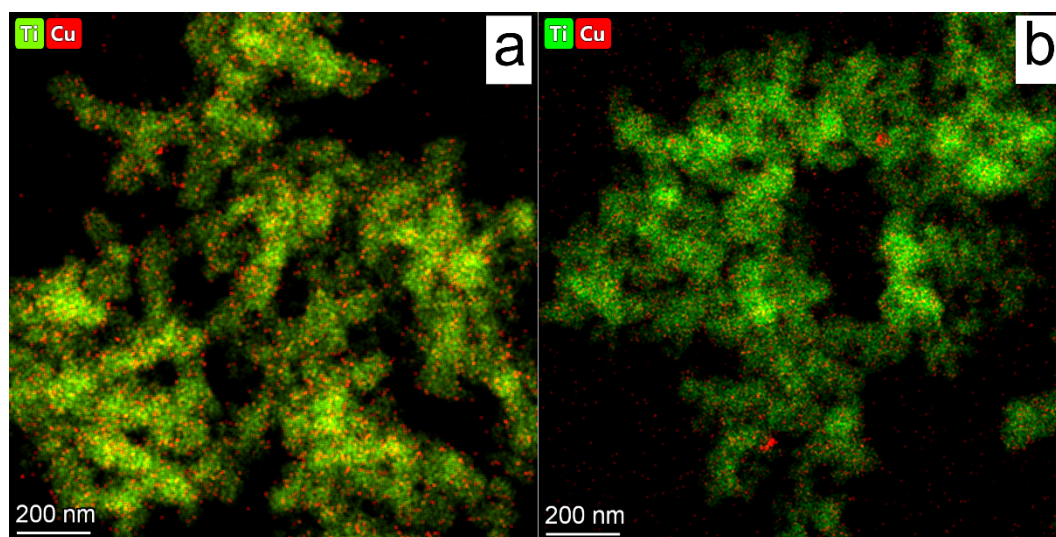


**Figure 8.** EDX mapping of (a) fresh Cu/TiO<sub>2</sub> 700 sample and (b) after irradiation for 120 h or 5 runs under LED-400 nm.

The results reveal that the calcination of TiO<sub>2</sub> at 700 °C facilitates the deposition of well-dispersed cocatalyst particles and prevents Cu/CuO<sub>x</sub> aggregation during even 100 h of the photocatalytic reaction. This effect promotes the CH<sub>4</sub> formation rate rather than the formation of CO. Additionally, the presence of copper oxides provides increased adsorption of visible light by the photocatalyst, which is vital for carrying out the multielectron process of CO<sub>2</sub> reduction to CH<sub>4</sub> upon irradiation in the visible region.

#### 4. Conclusions

In this study, the influence of a cocatalyst and thermal activation of TiO<sub>2</sub>-based photocatalysts on the CO<sub>2</sub> reduction process was investigated. Platinized photocatalysts were shown to be more active in relation to the CH<sub>4</sub> formation under UV light irradiation, while Cu-containing ones demonstrated superior activity in CH<sub>4</sub> production upon irradiation with visible light. The maximum overall CO<sub>2</sub> reduction rate under UV irradiation was 2.8 μmol h<sup>-1</sup> g<sup>-1</sup>, which was achieved over TiO<sub>2</sub> calcinated at 700 °C and modified with

Pt. The Cu/TiO<sub>2</sub> showed an activity rate of 2.6 μmol h<sup>-1</sup> g<sup>-1</sup>. The highest CO<sub>2</sub> reduction rate was 37 μmol h<sup>-1</sup> g<sup>-1</sup>, achieved over Cu/TiO<sub>2</sub> under light irradiation with a maximum intensity of 400 nm. At 425 nm, the Cu/TiO<sub>2</sub> 700 demonstrated a maximum CO<sub>2</sub> reduction rate of 11 μmol h<sup>-1</sup> g<sup>-1</sup>. Both rates are high, compared with the published data on CO<sub>2</sub> reduction over different photocatalysts [3,55,56]. Under purely visible light irradiation (LED-425 nm), AQE and S(CH<sub>4</sub>) for Cu/TiO<sub>2</sub> 700 photocatalyst were achieved by 0.23% and 90%, respectively. Therefore, the replacement of platinum with copper is an effective method for the synthesis of a visible active photocatalyst for CO<sub>2</sub> reduction, provided that calcined TiO<sub>2</sub> (700 °C) is used.

The stability of Cu/TiO<sub>2</sub> 700 was tested during 120 h of reaction under LED-400 nm. It was shown that the cocatalyst particles began to aggregate during experiments, but this process proceeded much more slowly on the surface of calcined TiO<sub>2</sub>. Platinum was in the metallic state on the surface of both TiO<sub>2</sub> and TiO<sub>2</sub> 700 samples. Copper was present in various states, and the Cu/TiO<sub>2</sub> 700 sample contained less Cu<sup>2+</sup> than Cu/TiO<sub>2</sub>, but this sample had a uniform distribution of cocatalyst, which is beneficial for the CH<sub>4</sub> production under irradiation of visible light. This photocatalyst demonstrated fairly good stability over 120 h of CO<sub>2</sub> reduction. A slight decrease in the CH<sub>4</sub> formation rate is probably associated with the beginning enlargement of Cu/CuO<sub>x</sub> particles and the reduction of copper oxides to metal particles, which reduces light absorption in the visible region.

**Supplementary Materials:** The following supporting information can be downloaded at: <https://www.mdpi.com/article/10.3390/nano12091584/s1>, Figure S1: Pt4f core-level spectra of the fresh (a) Pt-TiO<sub>2</sub> photocatalysts and after irradiation (b) under LED-400 nm. The spectra are normalized to the integral intensity of the corresponding Ti2p core-level spectra. Figure S2: EDX mapping (in HAADF STEM mode) of the fresh Cu/TiO<sub>2</sub> (a) catalyst and after irradiation (b,c) for 24 h under LED-450 nm. Figure S3: Cu2p core-level spectra of the fresh (a) Cu-TiO<sub>2</sub> photocatalysts and after irradiation (b) under LED-400 nm. Figure S4: EDX mapping (in HAADF STEM mode) of the Cu/TiO<sub>2</sub> 700 catalyst after irradiation for 120 h under LED-400 nm (Cu (a), O (b)).

**Author Contributions:** Investigation, data curation, visualization, writing—original draft preparation, funding acquisition, project administration, A.A.S.; investigation, data curation, visualization, writing—original draft preparation, A.Y.K.; investigation, data curation, E.Y.G.; writing—original draft preparation, supervision, conceptualization, project administration, E.A.K. All authors have read and agreed to the published version of the manuscript.

**Funding:** This study was supported by Russian Science Foundation (Grant #21-73-10235).

**Data Availability Statement:** The data presented in this study are available on request from the corresponding author.

**Acknowledgments:** The XPS and HR TEM experiments were performed using the facilities of the shared research center “National Center of Investigation of Catalysts” at Boreskov Institute of Catalysis. The authors are grateful to T. Larina for the UV-Vis measurements and D. Vasilchenko for the LED emission spectra measurements.

**Conflicts of Interest:** The authors declare no conflict of interest.

## References

1. Christoforidis, K.C.; Fornasiero, P. Photocatalysis for Hydrogen Production and CO<sub>2</sub> Reduction: The Case of Copper-Catalysts. *ChemCatChem* **2019**, *11*, 368–382. [[CrossRef](#)]
2. Yaashikaa, P.R.; Senthil Kumar, P.; Varjani, S.J.; Saravanan, A. A review on photochemical, biochemical and electrochemical transformation of CO<sub>2</sub> into value-added products. *J. CO<sub>2</sub> Util.* **2019**, *33*, 131–147. [[CrossRef](#)]
3. Kozlova, E.A.; Lyulyukin, M.N.; Kozlov, D.V.; Parmon, V.N. Semiconductor photocatalysts and mechanisms of carbon dioxide reduction and nitrogen fixation under UV and visible light. *Russ. Chem. Rev.* **2021**, *90*, 1520–1543. [[CrossRef](#)]
4. Shehzad, N.; Tahir, M.; Johari, K.; Murugesan, T.; Hussain, M. A critical review on TiO<sub>2</sub> based photocatalytic CO<sub>2</sub> reduction system: Strategies to improve efficiency. *J. CO<sub>2</sub> Util.* **2018**, *26*, 98–122. [[CrossRef](#)]
5. Meryem, S.S.; Nasreen, S.; Siddique, M.; Khan, R. An overview of the reaction conditions for an efficient photoconversion of CO<sub>2</sub>. *Rev. Chem. Eng.* **2018**, *34*, 409–425. [[CrossRef](#)]

6. Hoffmann, M.R.; Martin, S.T.; Choi, W.; Bahnemann, D.W. Environmental Applications of Semiconductor Photocatalysis. *Chem. Rev.* **1995**, *95*, 69–96. [[CrossRef](#)]
7. Wang, Z.; Fan, J.; Cheng, B.; Yu, J.; Xu, J. Nickel-based cocatalysts for photocatalysis: Hydrogen evolution, overall water splitting and CO<sub>2</sub> reduction. *Mater. Today Phys.* **2020**, *15*, 100279. [[CrossRef](#)]
8. Habisreutinger, S.N.; Schmidt-Mende, L.; Stolarczyk, J.K. Photocatalytic Reduction of CO<sub>2</sub> on TiO<sub>2</sub> and Other Semiconductors. *Angew. Chemie Int. Ed.* **2013**, *52*, 7372–7408. [[CrossRef](#)]
9. Ran, J.; Jaroniec, M.; Qiao, S.Z. Cocatalysts in Semiconductor-based Photocatalytic CO<sub>2</sub> Reduction: Achievements, Challenges, and Opportunities. *Adv. Mater.* **2018**, *30*, 1704649. [[CrossRef](#)]
10. Lettieri, S.; Pavone, M.; Fioravanti, A.; Amato, L.S.; Maddalena, P. Charge Carrier Processes and Optical Properties in TiO<sub>2</sub> and TiO<sub>2</sub>-Based Heterojunction Photocatalysts: A Review. *Materials* **2021**, *14*, 1645. [[CrossRef](#)]
11. Tu, W.; Zhou, Y.; Zou, Z. Photocatalytic Conversion of CO<sub>2</sub> into Renewable Hydrocarbon Fuels: State-of-the-Art Accomplishment, Challenges, and Prospects. *Adv. Mater.* **2014**, *26*, 4607–4626. [[CrossRef](#)]
12. Yin, M.; Wu, C.K.; Lou, Y.; Burda, C.; Koberstein, J.T.; Zhu, Y.; O'Brien, S. Copper oxide nanocrystals. *J. Am. Chem. Soc.* **2005**, *127*, 9506–9511. [[CrossRef](#)]
13. Yu, J.; Hai, Y.; Jaroniec, M. Photocatalytic hydrogen production over CuO-modified titania. *J. Colloid Interface Sci.* **2011**, *357*, 223–228. [[CrossRef](#)] [[PubMed](#)]
14. Meshram, S.P.; Adhyapak, P.V.; Mulik, U.P.; Amalnerkar, D.P. Facile synthesis of CuO nanomorphs and their morphology dependent sunlight driven photocatalytic properties. *Chem. Eng. J.* **2012**, *204–206*, 158–168. [[CrossRef](#)]
15. Zoolfakar, A.S.; Rani, R.A.; Morfa, A.J.; O'Mullane, A.P.; Kalantar-Zadeh, K. Nanostructured copper oxide semiconductors: A perspective on materials, synthesis methods and applications. *J. Mater. Chem. C* **2014**, *2*, 5247–5270. [[CrossRef](#)]
16. Florica, C.; Costas, A.; Preda, N.; Beregoi, M.; Kuncser, A.; Apostol, N.; Popa, C.; Socol, G.; Diculescu, V.; Enculescu, I. Core-shell nanowire arrays based on ZnO and Cu<sub>x</sub>O for water stable photocatalysts. *Sci. Rep.* **2019**, *9*, 17268. [[CrossRef](#)] [[PubMed](#)]
17. Markovskaya, D.V.; Zhurenok, A.V.; Kurenkova, A.Y.; Kremneva, A.M.; Saraev, A.A.; Zharkov, S.M.; Kozlova, E.A.; Kaichev, V.V. New titania-based photocatalysts for hydrogen production from aqueous-alcoholic solutions of methylene blue. *RSC Adv.* **2020**, *10*, 34137–34148. [[CrossRef](#)]
18. Asahi, R.; Morikawa, T.; Irie, H.; Ohwaki, T. Nitrogen-doped titanium dioxide as visible-light-sensitive photocatalyst: Designs, developments, and prospects. *Chem. Rev.* **2014**, *114*, 9824–9852. [[CrossRef](#)]
19. Lepadatu, A.M.; Slav, A.; Palade, C.; Dascalescu, I.; Enculescu, M.; Iftimie, S.; Lazanu, S.; Teodorescu, V.S.; Ciurea, M.L.; Stoica, T. Dense Ge nanocrystals embedded in TiO<sub>2</sub> with exponentially increased photoconduction by field effect. *Sci. Rep.* **2018**, *8*, 4898. [[CrossRef](#)]
20. Khan, M.M.; Ansari, S.A.; Pradhan, D.; Ansari, M.O.; Han, D.H.; Lee, J.; Cho, M.H. Band gap engineered TiO<sub>2</sub> nanoparticles for visible light induced photoelectrochemical and photocatalytic studies. *J. Mater. Chem. A* **2014**, *2*, 637–644. [[CrossRef](#)]
21. Ansari, S.A.; Cho, M.H. Highly Visible Light Responsive, Narrow Band gap TiO<sub>2</sub> Nanoparticles Modified by Elemental Red Phosphorus for Photocatalysis and Photoelectrochemical Applications. *Sci. Rep.* **2016**, *6*, 25405. [[CrossRef](#)] [[PubMed](#)]
22. Zhou, R.; Li, D.; Qu, B.; Sun, X.; Zhang, B.; Zeng, X.C. Rutile TiO<sub>2</sub>(011)-2 × 1 Reconstructed Surfaces with Optical Absorption over the Visible Light Spectrum. *ACS Appl. Mater. Interfaces* **2016**, *8*, 27403–27410. [[CrossRef](#)] [[PubMed](#)]
23. Maldonado, M.I.; López-Martín, A.; Colón, G.; Peral, J.; Martínez-Costa, J.I.; Malato, S. Solar pilot plant scale hydrogen generation by irradiation of Cu/TiO<sub>2</sub> composites in presence of sacrificial electron donors. *Appl. Catal. B Environ.* **2018**, *229*, 15–23. [[CrossRef](#)]
24. Kurenkova, A.Y.; Kremneva, A.M.; Saraev, A.A.; Murzin, V.; Kozlova, E.A.; Kaichev, V.V. Influence of Thermal Activation of Titania on Photoreactivity of Pt/TiO<sub>2</sub> in Hydrogen Production. *Catal. Lett.* **2021**, *151*, 748–754. [[CrossRef](#)]
25. Kozlova, E.A.; Kurenkova, A.Y.; Gerasimov, E.Y.; Gromov, N.V.; Medvedeva, T.B.; Saraev, A.A.; Kaichev, V.V. Comparative study of photoreforming of glycerol on Pt/TiO<sub>2</sub> and CuO<sub>x</sub>/TiO<sub>2</sub> photocatalysts under UV light. *Mater. Lett.* **2021**, *283*, 128901. [[CrossRef](#)]
26. Scofield, J.H. Hartree-Slater subshell photoionization cross-sections at 1254 and 1487 eV. *J. Electron. Spectros. Relat. Phenomena* **1976**, *8*, 129–137. [[CrossRef](#)]
27. Fairley, N. CasaXPS Software. Available online: <https://www.casaxps.com> (accessed on 10 April 2022).
28. Bickley, R.I.; Gonzalez-Carreño, T.; Lees, J.S.; Palmisano, L.; Tilley, R.J.D. A structural investigation of titanium dioxide photocatalysts. *J. Solid State Chem.* **1991**, *92*, 178–190. [[CrossRef](#)]
29. Leung, D.Y.C.; Fu, X.; Wang, C.; Ni, M.; Leung, M.K.H.; Wang, X.; Fu, X. Hydrogen production over titania-based photocatalysts. *ChemSusChem* **2010**, *3*, 681–694. [[CrossRef](#)]
30. Yu, J.; Qi, L.; Jaroniec, M. Hydrogen production by photocatalytic water splitting over Pt/TiO<sub>2</sub> nanosheets with exposed (001) facets. *J. Phys. Chem. C* **2010**, *114*, 13118–13125. [[CrossRef](#)]
31. Cheng, S.P.; Wei, L.W.; Wang, H.P. Photocatalytic Reduction of CO<sub>2</sub> to Methanol by Cu<sub>2</sub>O/TiO<sub>2</sub> Heterojunctions. *Sustainability* **2022**, *14*, 374. [[CrossRef](#)]
32. Khiavi, N.D.; Katal, R.; Eshkalak, S.K.; Masudy-Panah, S.; Ramakrishna, S.; Jiangyong, H. Visible Light Driven Heterojunction Photocatalyst of CuO–Cu<sub>2</sub>O Thin Films for Photocatalytic Degradation of Organic Pollutants. *Nanomaterials* **2019**, *9*, 1011. [[CrossRef](#)] [[PubMed](#)]
33. Chiang, K.; Amal, R.; Tran, T. Photocatalytic degradation of cyanide using titanium dioxide modified with copper oxide. *Adv. Environ. Res.* **2002**, *6*, 471–485. [[CrossRef](#)]

34. Lyulyukin, M.N.; Kurenkova, A.Y.; Bukhtiyarov, A.V.; Kozlova, E.A. Carbon dioxide reduction under visible light: A comparison of cadmium sulfide and titania photocatalysts. *Mendeleev Commun.* **2020**, *30*, 192–194. [[CrossRef](#)]
35. Ghosh, S.; Nambissan, P.M.G. Evidence of oxygen and Ti vacancy induced ferromagnetism in post-annealed undoped anatase TiO<sub>2</sub> nanocrystals: A spectroscopic analysis. *J. Solid State Chem.* **2019**, *275*, 174–180. [[CrossRef](#)]
36. Fedorov, A.; Saraev, A.; Kremneva, A.; Selivanova, A.; Vorokhta, M.; Šmíd, B.; Bulavchenko, O.; Yakovlev, V.; Kaichev, V. Kinetic and mechanistic study of CO oxidation over nanocomposite Cu–Fe–Al oxide catalysts. *ChemCatChem* **2020**, *12*, 4911–4921. [[CrossRef](#)]
37. Fu, J.; Jiang, K.; Qiu, X.; Yu, J.; Liu, M. Product selectivity of photocatalytic CO<sub>2</sub> reduction reactions. *Mater. Today* **2020**, *32*, 222–243. [[CrossRef](#)]
38. Li, Y.; Wang, W.N.; Zhan, Z.; Woo, M.H.; Wu, C.Y.; Biswas, P. Photocatalytic reduction of CO<sub>2</sub> with H<sub>2</sub>O on mesoporous silica supported Cu/TiO<sub>2</sub> catalysts. *Appl. Catal. B Environ.* **2010**, *100*, 386–392. [[CrossRef](#)]
39. Usubharatana, P.; McMartin, D.; Veawab, A.; Tontiwachwuthikul, P. Photocatalytic Process for CO<sub>2</sub> Emission Reduction from Industrial Flue Gas Streams. *Ind. Eng. Chem. Res.* **2006**, *45*, 2558–2568. [[CrossRef](#)]
40. Vitiello, G.; Clarizia, L.; Abdelraheem, W.; Esposito, S.; Bonelli, B.; Ditaranto, N.; Vergara, A.; Nadagouda, M.; Dionysiou, D.D.; Andreozzi, R.; et al. Near UV-Irradiation of CuO<sub>x</sub>-Impregnated TiO<sub>2</sub> Providing Active Species for H<sub>2</sub> Production Through Methanol Photoreforming. *ChemCatChem* **2019**, *11*, 4314–4326. [[CrossRef](#)]
41. Karamian, E.; Sharifnia, S. On the general mechanism of photocatalytic reduction of CO<sub>2</sub>. *J. CO<sub>2</sub> Util.* **2016**, *16*, 194–203. [[CrossRef](#)]
42. Shi, Q.; Ping, G.; Wang, X.; Xu, H.; Li, J.; Cui, J.; Abroshan, H.; Ding, H.; Li, G. CuO/TiO<sub>2</sub> heterojunction composites: An efficient photocatalyst for selective oxidation of methanol to methyl formate. *J. Mater. Chem. A* **2019**, *7*, 2253–2260. [[CrossRef](#)]
43. Nishikiori, H.; Harata, N.; Yamaguchi, S.; Ishikawa, T.; Kondo, H.; Kikuchi, A.; Yamakami, T.; Teshima, K. Formation of CuO on TiO<sub>2</sub> Surface Using its Photocatalytic Activity. *Catalysts* **2019**, *9*, 383. [[CrossRef](#)]
44. Preda, N.; Costas, A.; Beregoi, M.; Apostol, N.; Kuncser, A.; Curutiu, C.; Iordache, F.; Enculescu, I. Functionalization of eggshell membranes with CuO–ZnO based p–n junctions for visible light induced antibacterial activity against Escherichia coli. *Sci. Rep.* **2020**, *10*, 20960. [[CrossRef](#)] [[PubMed](#)]
45. Wei, T.; Zhu, Y.N.; An, X.; Liu, L.M.; Cao, X.; Liu, H.; Qu, J. Defect Modulation of Z-Scheme TiO<sub>2</sub>/Cu<sub>2</sub>O Photocatalysts for Durable Water Splitting. *ACS Catal.* **2019**, *9*, 8346–8354. [[CrossRef](#)]
46. Lv, S.; Wang, Y.; Zhou, Y.; Liu, Q.; Song, C.; Wang, D. Oxygen vacancy stimulated direct Z-scheme of mesoporous Cu<sub>2</sub>O/TiO<sub>2</sub> for enhanced photocatalytic hydrogen production from water and seawater. *J. Alloys Compd.* **2021**, *868*, 159144. [[CrossRef](#)]
47. Zhang, Y.; Zhao, J.; Wang, H.; Xiao, B.; Zhang, W.; Zhao, X.; Lv, T.; Thangamuthu, M.; Zhang, J.; Guo, Y.; et al. Single-atom Cu anchored catalysts for photocatalytic renewable H<sub>2</sub> production with a quantum efficiency of 56%. *Nat. Commun.* **2022**, *13*, 58. [[CrossRef](#)]
48. Sun, Z.; Fang, W.; Zhao, L.; Wang, H. 3D porous Cu-NPs/g-C<sub>3</sub>N<sub>4</sub> foam with excellent CO<sub>2</sub> adsorption and Schottky junction effect for photocatalytic CO<sub>2</sub> reduction. *Appl. Surf. Sci.* **2020**, *504*, 144347. [[CrossRef](#)]
49. Mekasuwandumrong, O.; Jantarasorn, N.; Panpranot, J.; Ratova, M.; Kelly, P.; Praserttham, P. Synthesis of Cu/TiO<sub>2</sub> catalysts by reactive magnetron sputtering deposition and its application for photocatalytic reduction of CO<sub>2</sub> and H<sub>2</sub>O to CH<sub>4</sub>. *Ceram. Int.* **2019**, *45*, 22961–22971. [[CrossRef](#)]
50. Lan, Y.; Xie, Y.; Chen, J.; Hu, Z.; Cui, D. Selective photocatalytic CO<sub>2</sub> reduction on copper-titanium dioxide: A study of the relationship between CO production and H<sub>2</sub> suppression. *Chem. Commun.* **2019**, *55*, 8068–8071. [[CrossRef](#)]
51. Bulavchenko, O.A.; Vinokurov, Z.S.; Saraev, A.A.; Tsapina, A.M.; Trigub, A.L.; Gerasimov, E.Y.; Gladky, A.Y.; Fedorov, A.V.; Yakovlev, V.A.; Kaichev, V. V The Influence of Cu and Al Additives on Reduction of Iron(III) Oxide: In Situ XRD and XANES Study. *Inorg. Chem.* **2019**, *58*, 4842–4850. [[CrossRef](#)]
52. Xing, H.; Lei, E.; Guo, Z.; Zhao, D.; Li, X.; Liu, Z. Exposing the photocorrosion mechanism and control strategies of a CuO photocathode. *Inorg. Chem. Front.* **2019**, *6*, 2488–2499. [[CrossRef](#)]
53. Monte, M.; Gamarra, D.; López Cámara, A.; Rasmussen, S.B.; Gyorffy, N.; Schay, Z.; Martínez-Arias, A.; Conesa, J.C. Preferential oxidation of CO in excess H<sub>2</sub> over CuO/CeO<sub>2</sub> catalysts: Performance as a function of the copper coverage and exposed face present in the CeO<sub>2</sub> support. *Catal. Today* **2014**, *229*, 104–113. [[CrossRef](#)]
54. Fierro, G.; Lo Jacono, M.; Inversi, M.; Dragone, R.; Porta, P. TPR and XPS study of cobalt–copper mixed oxide catalysts: Evidence of a strong Co–Cu interaction. *Top. Catal.* **2000**, *10*, 39–48. [[CrossRef](#)]
55. Barrocas, B.T.; Ambrožová, N.; Kočí, K. Photocatalytic Reduction of Carbon Dioxide on TiO<sub>2</sub> Heterojunction Photocatalysts; A Review. *Materials* **2022**, *15*, 967. [[CrossRef](#)]
56. Sun, N.; Zhu, Y.; Li, M.; Zhang, J.; Qin, J.; Li, Y.; Wang, C. Thermal coupled photocatalysis over Pt/g-C<sub>3</sub>N<sub>4</sub> for selectively reducing CO<sub>2</sub> to CH<sub>4</sub> via cooperation of the electronic metal–support interaction effect and the oxidation state of Pt. *Appl. Catal. B Environ.* **2021**, *298*, 120565. [[CrossRef](#)]